ELSEVIER

Journal of Fluids and Structures 21 (2005) 65–74

JOURNAL OF FLUIDS AND STRUCTURES

www.elsevier.com/locate/jfs

Vortex shedding and galloping of open semi-circular and parabolic cylinders in cross-flow

D.S. Weaver[a,*], I. Veljkovic[b]

[a]*Department of Mechanical Engineering, McMaster University, Hamilton, ON, Canada L8S 4L7*
[b]*Pratt and Whitney Canada, Mississauga, ON, Canada*

Received 1 October 2004; accepted 3 June 2005

Abstract

An experimental wind-tunnel study was undertaken to investigate the flow-induced vibration behaviour of open semi-circular and parabolic cylinders in cross-flow. The motivation for the research was to investigate the cause of the fatigue failures of a number of parabolic section rotary mixing blades in a large mixing vessel. Results are presented for force coefficients as a function of angle of incidence of the flow, Strouhal number and amplitude response. It is shown that the parabolic cylinder is subject to large amplitude vortex shedding resonance and, when the elastic axis is sufficiently downstream of the section's centre of gravity, galloping instability.

1. Introduction

The research reported in this paper was motivated by the failure of a number of large mixing vessel blades. These blades were cantilevered parabolic cylinders with their open surface facing the direction of rotation so that they behaved like bluff bodies as well as radial pump impellers, as shown schematically in Fig. 1. Finite element analysis showed that the first cantilever mode of vibration predicted dynamic stresses which were largest at the point of fatigue crack initiation observed on the failed mixing blades (Veljkovic, 2002). It appears that the failures were caused by flow-induced vibration and, since there appeared to be no references in the open literature to flow-excitation of open parabolic cylinders, an experimental wind-tunnel study was undertaken.

It is well known that bluff bodies in cross-flow are subject to vortex shedding and, in some cases, galloping [see for example, Blevins (1990) and Naudascher and Rockwell (1994)]. Vortex shedding resonance occurs when the frequency of vortex shedding coincides with a natural frequency of the structure. The resonant amplitude depends on the so-called "mass-damping parameter" and, if the amplitude is sufficiently large, the vortex shedding becomes controlled by the structural motion in a strongly nonlinear process called "lock-in". On the other hand, galloping is a self-excited vibration in which the structure's motion induces lift forces in phase with, and dependent on, the velocity of the structure transverse to the flow direction. If the slope of the lift coefficient curve with respect to the angle of incidence of the relative flow velocity is negative, a negative damping force is generated which may overcome the structural damping and lead to dynamic instability (Den Hartog, 1956). Thus, structural damping affects the onset velocity for galloping instability. Furthermore, the after-body shape significantly influences the flow reattachment, and galloping may occur

*Corresponding author. Tel.: +1 905 525 9140; fax: +1 905 572 7944.
E-mail address: wearverds@mcmaster.ca (D.S. Weaver).

0889-9746/$ - see front matter © 2005 Elsevier Ltd. All rights reserved.
doi:10.1016/j.jfluidstructs.2005.06.004

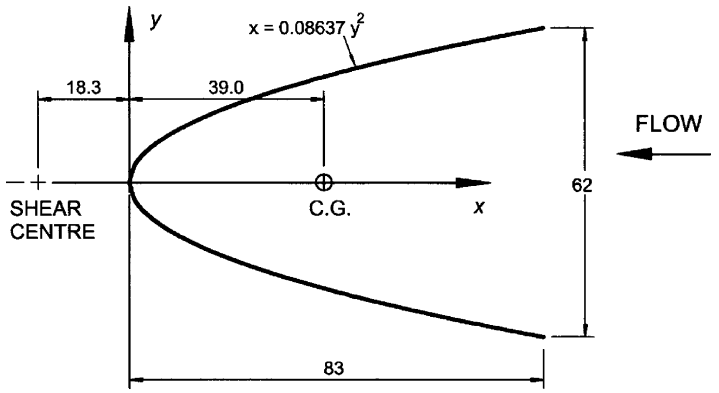

Fig. 1. Cross-section of parabolic model. All dimensions in mm.

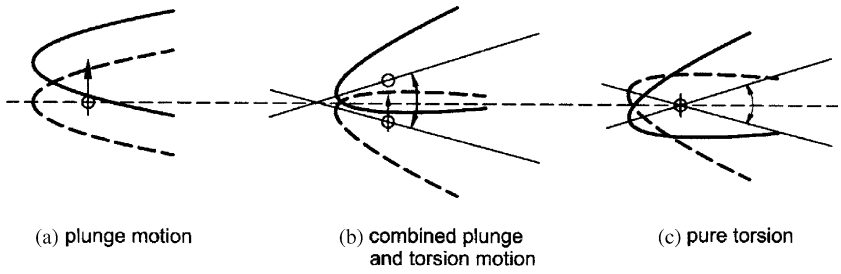

Fig. 2. Schematic representation of cross-sectional motion in different modes.

from rest (soft oscillator) or may require a significant disturbance from the body's rest position (hard oscillator). An example of a soft oscillator is a square-section cylinder (Novak, 1972), while a D-shaped section with its flat surface facing upstream is a hard oscillator (Novak and Tanaka, 1974).

Much research has been carried out on the galloping of cylindrical bluff bodies as summarized by Naudascher and Rockwell (1994). Most attention has been paid to bodies for which the elastic axis and centre of gravity coincide. Thus, the plunge motion (lift direction translation), Fig. 2(a), and torsional motion, Fig. 2(c) are mechanically uncoupled. In contrast, the parabolic cylinder of interest in the present study has its centre of gravity upstream of its shear centre (elastic axis) and, therefore, its natural frequencies consist of a combination of translation and rotation, Fig. 2(b). The study of a structural angle section by Modi and Slater (1983, 1994) is probably the bluff body shape published in the open literature which is most relevant to the present study. However, these authors suspended rigid angle models such that their translational and rotational natural frequencies were mechanically independent and different by a factor of about 3. Thus, they found independent plunge and torsional vortex shedding resonances with strong "lock-in" for the plunge mode and essentially no lock-in for the torsional mode. They also found plunge mode galloping which, for small damping, appeared to nearly coincide with vortex shedding resonance. Interestingly, they also observed small rotational motion in phase with the plunge motion at the plunge mode frequency during galloping, indicating some form of mode coupling. Furthermore, doubling the damping very substantially delayed the onset of galloping so that this was well separated from the vortex shedding resonances in the plunge and torsional modes (Modi and Slater, 1994). While very interesting, the removal of the mechanical (dynamic) coupling of the plunge and torsional modes in this study makes it difficult to relate the results to the practical problem.

This paper presents the results of a wind tunnel study of the flow-induced vibrations of an open parabolic cylinder in cross-flow. Open and closed semi-circular cylinders were studied to establish the effect of the open geometry when compared with a solid cylinder, and to provide a comparative basis for the parabolic cylinder study. The cylinder supports were designed such that the elastic axis could be adjusted relative to the centre of gravity. Results are presented for force coefficients, Strouhal number and cylinder response. The response behaviour is examined for the cases where the elastic axis and centre of gravity are coincident (mechanically uncoupled) and for the elastic axis downstream of the centre of gravity (transverse and torsional modes coupled).

2. Experimental facility and model

The actual flow conditions seen by a mixing impeller blade in a mixing vessel are highly complex, certainly three-dimensional and turbulent. However, if the impeller blade is excited to periodic transverse vibrations at sufficient amplitudes to cause fatigue failure, then there must exist coherent flow structures roughly on the scale of the blade length. Furthermore, the flow parallel to the longitudinal axis of the blade is not likely to contribute in any essential way to the transverse motions of the blade. Thus, the use of a two-dimensional model should capture the essential features of the flow excitation phenomena while greatly simplifying the experiments. In keeping with this idealization is the use of a low-turbulence flow. It is known that turbulence can have an appreciable effect on transverse fluid force coefficients (and therefore galloping) depending upon afterbody shape, and may even change the nature of the instability (Novak, 1972; Novak and Tanaka, 1974; Nakamura and Tomonari, 1977; Nakamura and Yoshimura, 1982). Ambient turbulence levels can either raise or lower the stability threshold and the effect depends on the turbulence characteristics of the flow as well as after-body shape. Turbulence data were not available for the mixing vessel in question. Thus, idealized experiments were carried out in a low turbulence ($<1\%$) wind tunnel with a flow velocity range 0–30 m/s. The 2 m long octagonal test-section is 0.61 m between parallel sides and has a central 0.70 m section which can be removed for insertion of various models.

The parabolic model, shown in cross-section in Fig. 1, is a parabolic shaped cylinder given by $x = 0.0837y^2$, scaled geometrically from the mixing vessel blade. The overall test-section and model arrangement is shown in Fig. 3 and the square bracketed numbers in the following description correspond to the circled numbers in the figure. To ensure minimum weight with adequate stiffness, the model [1] was made from 1 mm plywood formed over 5 precision-machined 4.5 mm plywood bulkheads located equal distances apart by seven 2×4 mm hardwood stringers. The cylinder so formed was 0.57 m long and was fixed with 217 mm diameter end plates [2], leaving about 30 mm between the cylinder and the test-section sidewalls. The cylinder was fixed by rigid circular rods [3] at either end, located at the cylinder's centre of gravity. These rods passed through a hole in the test-section walls and were fixed to a light, stiff support beam [4] at each end in a way which permitted rotating the model to any fixed angle relative to the beam, and therefore, flow direction. These beams were attached to external rigid supports [6] by means of two 0.635×15 mm spring steel elastic beams [5] on each side. The length and location relative to the cylinder centre of gravity of the elastic beams could be varied so that the natural frequencies in the plunge and torsional modes as well as the location of the effective elastic axis could all be independently controlled. The total sprung mass of the model was 0.650 kg.

The model displacement as well as the lift force and moment coefficients were obtained using strain gauges [7] placed near the fixed supports on the elastic beams. The strain gauge signals were passed through a Wheatstone bridge and amplifier/signal conditioner to a dynamic signal analyser and data acquisition system. Calibration curves for

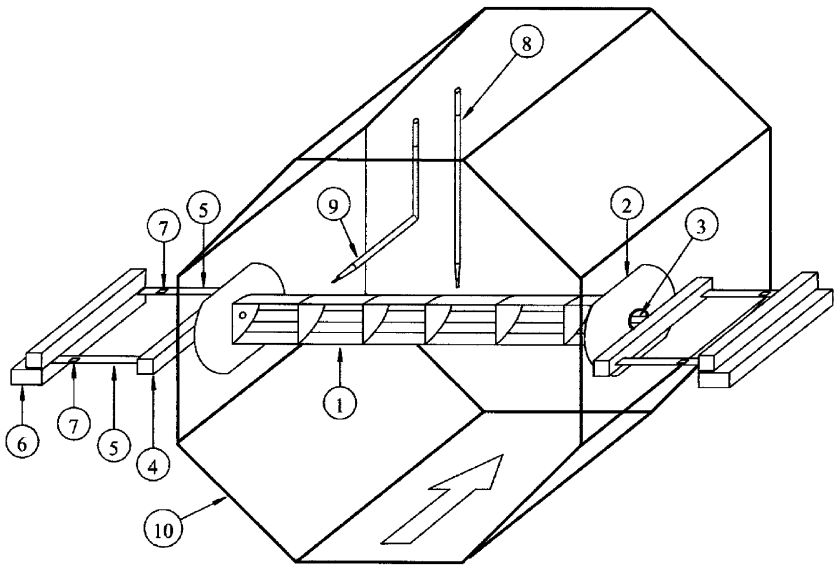

Fig. 3. Experimental model showing wind tunnel test-section and model suspension. 1. Test model, 2. end plate, 3. rigid model support rods, 4. stiff support beam, 5. elastic beams, 6. rigid support, 7. strain gauges, 8. wake response hot-wire probe, 9. flow velocity hot wire probe, 10. test-section.

displacement, force, and moment were obtained using static loading through a system of suspended weights. The calibration for displacement was linear up to a displacement of 6% of the characteristic length for the model, D, the cross-sectional opening dimension of 62 mm as seen in Fig. 1. For larger displacements, the elastic supports displayed nonlinear hardening. The maximum allowable displacement was $0.22D$, determined by the size of the cylinder support rod holes in the test-section walls.

Dynamic r.m.s. response amplitude measurements as well as measurements for the lift and moment coefficients (i.e., C_L and C_M) were obtained from the response power spectral density and the calibration curves. These were based on 50 sample averages with a frequency resolution of 0.25 Hz and the spectral peaks being integrated over ± 1.5 Hz about the cylinder natural frequency. The estimated uncertainty in the response measurements is less than 5% within the linear range of the elastic supports. The system damping was determined by computing the logarithmic decrement of damping from transient amplitude decay traces with no flow in the wind tunnel. The average of 5 such measurements gave a damping ratio of about 1% of critical. Flow velocity and wake response frequency were obtained using hot wire probes [8,9] and a constant temperature anemometer. The probes were carefully calibrated and the estimated uncertainty in flow velocity measurement is about 4% at a flow velocity of 6 m/s and lower for higher velocities.

The experimental set-up was evaluated by carrying out a series of experiments with a solid D-shape section cylinder as studied by Novak and Tanaka (1974). This was followed by another series of experiments with a cylinder of identical geometry but of open cross-section. In each case, the settings were identical to that described above for the open parabolic model.

3. Experimental results

3.1. Closed and open semi-circular sections

Several factors distinguish the open parabolic cylinder from previous studies: the separation of the elastic axis from the centre of gravity; the open nature of the cross-section; and the relative length of the after-body and its possible effects on the wake. Therefore, it was felt desirable to validate the experimental rig against published results while separating the effects of afterbody shape and mode coupling. The D-shaped section studied by Novak and Tanaka (1974) was selected and the behaviour of both the open and closed models were examined. In all these experiments with the semi-circular models, the elastic axis and centre of gravity were coincident, so that the plunge and torsional modes were mechanically uncoupled. The plunge mode frequency was about 13 Hz and the support arrangement was set up so that the torsional mode was equal to or greater than 40 Hz. The results are briefly presented below.

Fig. 4 shows the ratio of vortex shedding frequency to plunge mode natural frequency, and r.m.s. amplitude response normalized by the cylinder diameter, plotted against reduced velocity:

$$V_r = \frac{V}{f_n D}, \tag{1}$$

where V is the freestream velocity measured upstream of the model, D is the cylinder diameter, and f_n is the plunge mode natural frequency of the cylinder. Fig. 4(a) shows a clear linear relationship between the vortex shedding frequency, as measured by a hot wire in the cylinder wake, and the flow velocity, giving a Strouhal number of 0.15 ± 0.003. Fig. 4(b) shows a sharp resonance response to an r.m.s. amplitude of about 9% of D ($0.09D$) at a reduced velocity of about 6.7. The closed symbols represent data for the closed (solid) section while the open circles represent data for the thin-walled open section. Clearly, whether the cylinder section is open or closed has no effect on the vortex shedding or resonance response of the cylinder in the plunge mode. No galloping was observed, which is consistent with the findings of Novak and Tanaka (1974). A D-shaped section with its flat surface facing upstream is a "hard" oscillator and does not gallop from rest.

The lift force and torsional moment on the cylinder were measured as a function of incidence angle by fixing the cylinder at various angles over the range 0–180°, each experiment at a Reynolds number of 26,600. The lift coefficient, C_L, is defined as

$$C_L = \frac{2F_L}{\rho D L V^2}, \tag{2}$$

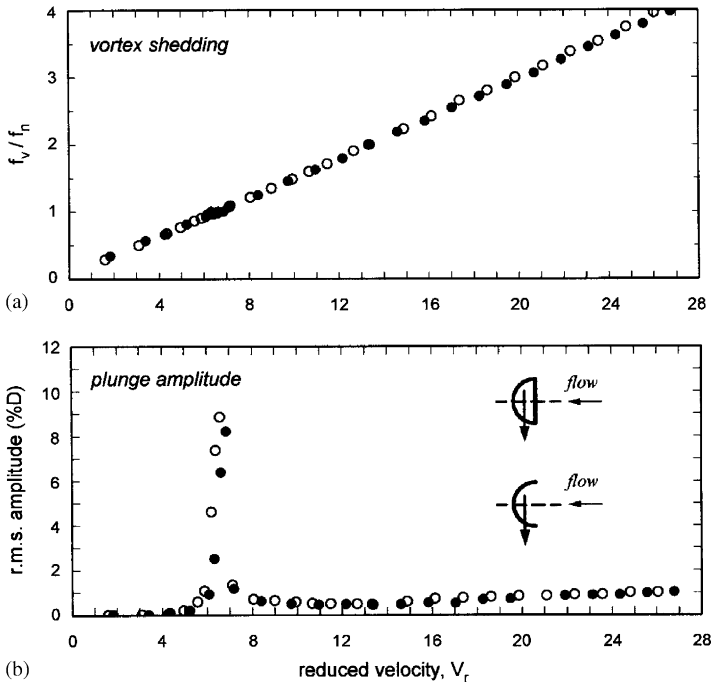

Fig. 4. Comparison of open and closed model response for the semi-circular cylinder: ●, solid model, $\mathrm{Re} = 10^5$; ○, open model, $\mathrm{Re} = 0.82 \times 10^5$.

where F_L is the measured lift force, L is the cylinder length and ρ is the density of air at the laboratory temperature. The moment coefficient, C_M, is defined as

$$C_M = \frac{2M}{\rho D^2 L V^2}, \tag{3}$$

where M is the measured aerodynamic moment on the cylinder. F_L and M were obtained from the strain gauge signals and the calibration curves. The lift and moment coefficients are plotted against angle of incidence in Fig. 5(a) and 5(b), respectively. Fig. 5(c) gives the Strouhal number, St, as a function of angle in incidence, where Strouhal number has not been corrected for the changing frontal projected length

$$\mathrm{St} = \frac{f_v D}{V}. \tag{4}$$

The solid symbols represent data from the solid model and, while Novak and Tanaka (1974) did not provide actual data, the present results agree with the Novak and Tanaka "smooth flow" curves within about 10%. It is well known that such data is dependent on ambient turbulence levels and, to some extent, Reynolds number. The Novak and Tanaka results were taken at a Reynolds number of 9×10^4 while the present data for the solid cylinder corresponds to a Reynolds number of 10^5. This comparison is considered to validate the present experimental procedure and to serve as a basis for establishing the effects of the open section and cylinder afterbody shape.

The open symbols in Fig. 5 are the data for the open semi-circular section, taken at a Reynolds number of 8.2×10^4. It is clear that for small angles of attack (less than about 30°), the openness of the semi-circular body has almost no effect on the force coefficients and the Strouhal number. As one would expect from examination of the body shape relative to the flow velocity direction, the largest effect of the openness of the body occurs between angles of attack $40^\circ \leqslant \alpha \leqslant 90^\circ$.

In summary, the semi-circular section at zero angle of attack exhibits a sharp resonance peak due to vortex shedding with a Strouhal number of 0.15 and a negative slope of the lift coefficient curve. Apparently, the slope of this curve is inadequate to produce galloping from rest. These results are not affected by changing the semi-circular body from a solid section to an open thin-walled shell.

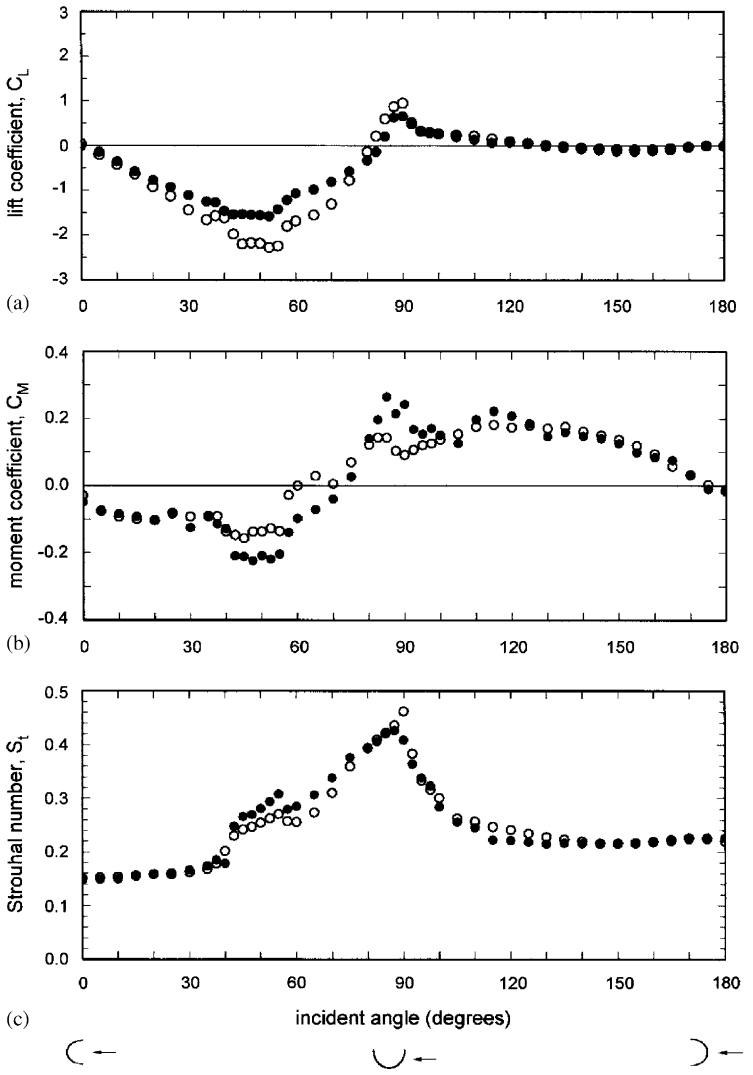

Fig. 5. Comparison of C_L, C_M and St for the open and solid semi-circular cylinder as a function of angle of attack: ● solid model, $\mathrm{Re} = 10^5$; ○, open model, $\mathrm{Re} = 0.82 \times 10^5$.

3.2. Parabolic section: elastic axis and centre of gravity coincident

A set of experiments were carried out with the elastic beams arranged symmetrically about the centre of gravity of the cylinder such that the plunge and torsion modes are independent. The effective length of the elastic beams was 65 mm and they were placed 269 mm apart on each side of the model. The plunge mode natural frequency was 13.5 Hz and the transverse "rocking mode" in the lift direction was 30.25 Hz. The torsional mode frequency was sufficiently high that it was not excited within the velocity range of the experiments.

The results for the dominant frequency and amplitude response are given in Fig. 6, plotted against reduced velocity. The dominant frequency in the wake and amplitude response spectra, f_v, Fig. 6(a), has been normalized using the plunge mode natural frequency, $f_n = 13.5$ Hz. The r.m.s. response amplitude, Fig. 6(b), has been normalized using the characteristic dimension, $D = 62$ mm, of the cylinder and presented as a percentage of D. These are all plotted against reduced velocity as defined by Eq. (1).

Fig. 6(a) shows a frequency response which is a linear function of flow velocity, characteristic of vortex shedding excitation. A least-squares fit of the data gives a Strouhal number of 0.13 ± 0.004 which was found to be independent of

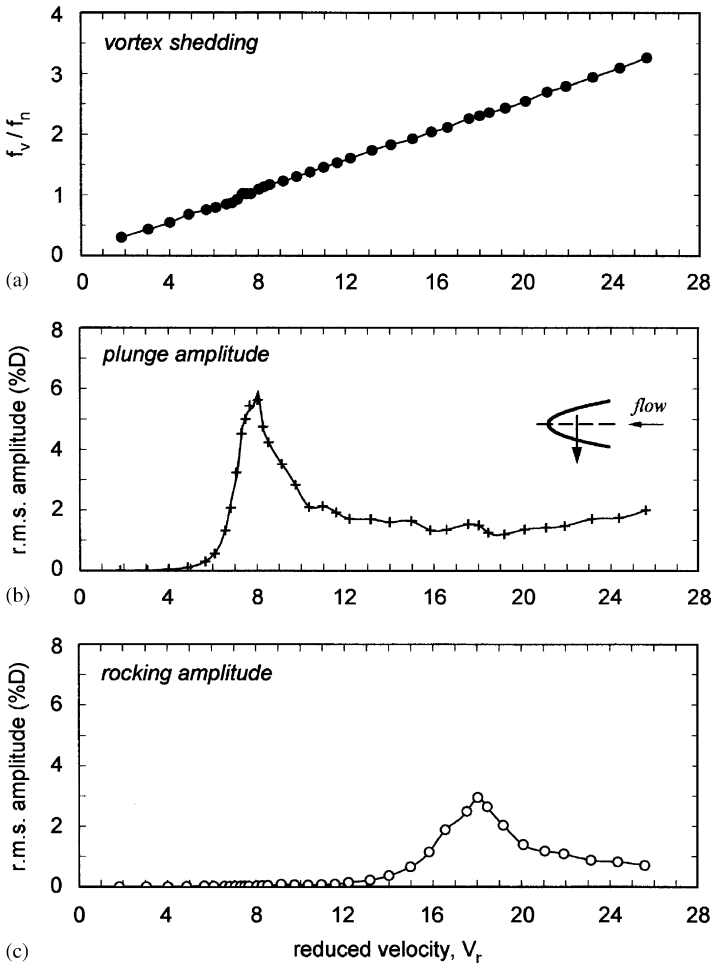

Fig. 6. Model with elastic axis and centre of gravity coincident. (a) Frequency ratio versus reduced velocity. (b) Plunge amplitude versus reduced velocity. (c) Rocking amplitude versus reduced velocity.

Reynolds number over the range 1.2×10^4–8.5×10^4. The graph also shows a small lock-in range at the plunge mode natural frequency, $f_v/f_n = 1$, corresponding to a reduced velocity of 7.69.

The plunge mode amplitude, Fig. 6(b), shows a steep rise at its resonant frequency, peaking to a value of about 5.8% of D. It seems clear that this motion is induced by vortex shedding resonance but the breadth of the peak suggests some more complex fluid-structure interaction. This behaviour is in contrast with the sharp vortex resonance peak observed for the D-shaped cylinder, Fig. 4(b), or the angle section with high damping (Modi and Slater, 1994). It is speculated that this behaviour is caused by the interaction of the wake with the after-body of the parabolic cylinder.

Fig. 6(c) shows the r.m.s. response amplitude in the rocking mode, 30.25 Hz, in the plunge direction. The peak occurs at a reduced velocity of about 18, just above that predicted for vortex shedding resonance in this mode, $V_r = 17.2$. The maximum r.m.s. displacement is 3% of D and Fig. 6(a) shows little evidence of lock-in. However, the breadth of this peak suggests that the response is more complex than simple resonance and that there may also be some interaction of the wake with the after-body.

As for the semi-circular cylinders, measurements were made of the lift force, moment and wake periodicity with the cylinder fixed at various angles of attack to the flow from 0° to 180°. This permitted the lift and moment coefficients to be computed using Eqs. (2) and (3), respectively, as well as the Strouhal number using Eq. (4). The results are plotted in Fig. 7(a)–(c).

It is seen in Fig. 7(a) that the shape of the lift coefficient curve is negative over the incidence angle range 0–30°, suggesting that some negative aerodynamic damping can be expected. Apparently, this was sufficient to substantially broaden the resonance response peak in Fig. 6(b) but not adequate to produce galloping. The moment coefficients in

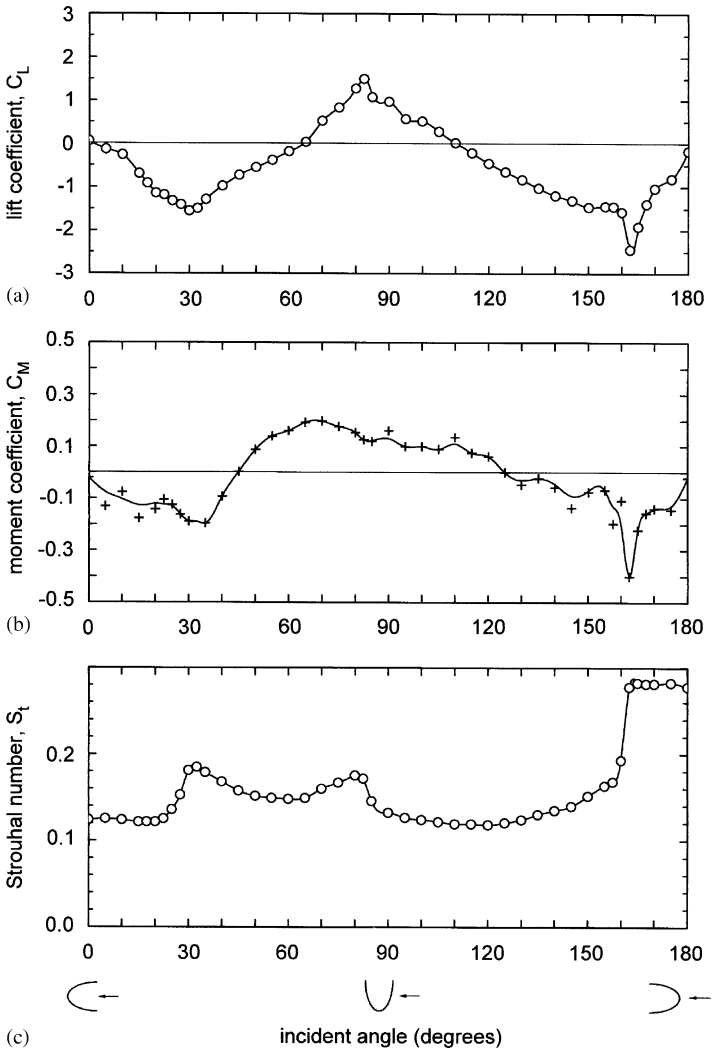

Fig. 7. Model with elastic axis and centre of gravity coincident: (a) lift coefficient versus incident angle; (b) moment coefficient versus incident angle; (c) Strouhal number versus incident angle.

Fig. 7(b) are relatively small and the scatter in the data is thought to be due to experimental uncertainty in the moment measurements. Nonetheless, the data show similar trends to those in Fig. 7(a). Peaks appear at angles of about 30°, 80°, and 165°, and each corresponds to an abrupt change in Strouhal number, Fig. 7(c). These are considered to be the result of sudden changes in wake interaction with the cylinder after-body and, to some extent at 30° and 80°, the effect of flow in and out of the open section.

3.3. Elastic axis behind the centre of gravity

The elastic suspension beams were located 94 mm apart with the centreline of the upstream beam about 43 mm downstream of the cylinder centre of gravity. The cylinder in this arrangement has 2 degrees of freedom with each mode involving translation and rotation of the centre of gravity. The fundamental mode was 9.0 Hz and had a node downstream of the cylinder centre of gravity as shown schematically in Fig. 2(b). Thus, this mode simulates the actual motion of the cantilever end of the mixing impeller blade.

Fig. 8 provides a plot of the amplitude response of the cylinder versus reduced velocity. It is seen that the cylinder develops galloping instability at a reduced velocity of about 6. The experiment was stopped when the model support rods began impacting their holes in the sides of the wind tunnel test-section, as indicated by the dashed line at $0.23D$. It

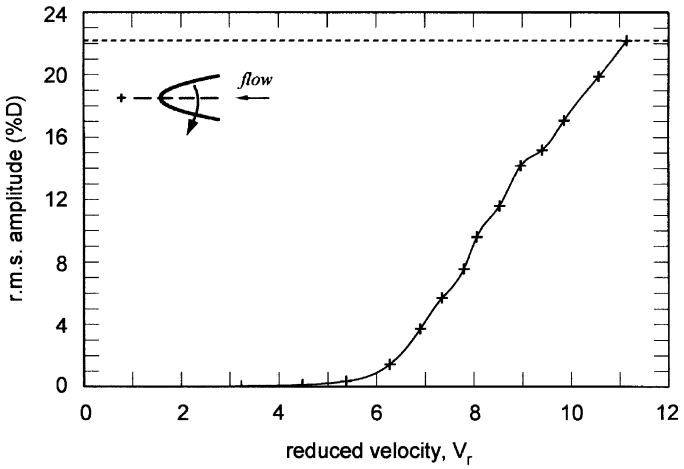

Fig. 8. Model with elastic axis downstream of centre of gravity: r.m.s. amplitude versus reduced velocity.

is interesting to note that, based upon a Strouhal number of 0.13 as indicated above, vortex shedding resonance is expected at a reduced velocity of about 7.7. Therefore, it appears that the parabolic cylinder in this arrangement is a "soft" oscillator, galloping from rest at a reduced velocity below that required for vortex shedding resonance.

4. Discussion

The motivation for the present study was to determine what flow excitation mechanism could have caused the failures of the mixing impeller blades in question. The experimental results show that an open parabolic shaped cylinder in combined translation and rotation is susceptible to galloping instability and suggest that this is the most likely cause of the observed blade failures However, the experiments were highly idealized (2-D model in a low turbulence flow) and much remains to be discovered regarding this phenomenon.

The afterbody shape influences vortex formation in the body wake and influences whether or not flow reattachment occurs. The latter is also strongly influenced by the angle of attack of the flow relative to the cylinder which, in turn, is affected by the velocity of the cylinder transverse to the mean flow direction and any rotational motion of the body. Since the open parabolic section would only gallop from rest when the centre of gravity was sufficiently far ahead of the elastic axis, it appears that some rotational motion of the cylinder is required for instability, at least in smooth flow. Ambient turbulence levels could also significantly affect the onset velocity for galloping. Future research should include parametric studies of the effects of varying the distance between the centre of gravity and the elastic axis to establish the limits required for galloping, varying the damping to separate the velocities at which vortex shedding resonance and galloping occur, and varying the level of free stream turbulence.

5. Conclusions

A series of wind tunnel experiments were carried out to study the flow-induced vibrations of open and solid semi-circular cylinders and an open parabolic cylinder in cross-flow. The motivation for this research was to determine the susceptibility of an open parabolic cylinder to vortex shedding resonance and/or galloping instability and, thereby, explain the cause of a number of mixing impeller blade failures. While the experiments were carried out using a 2-D model in a low turbulence wind tunnel, they did demonstrate that the blade failures were quite likely due to galloping instability. In addition, some general conclusions can be drawn from this research, as follows.

1. Experiments with the solid semi-circular cylinder verified previously published results and showed that this bluff body shape is subject to a sharp vortex shedding resonance response at a Strouhal number of 0.15. Such a body is a "hard" oscillator as it does not gallop from rest.

2. Experiments with the open semi-circular cylinder showed that such a change in geometry from a solid cylinder had essentially no effect on the vortex shedding, vortex shedding response, or the lift and moment coefficients for flow incident angle less than about 30°.
3. The parabolic cylinder with its elastic axis coincident with its centre of gravity is subject to strong vortex shedding with a Strouhal number of 0.13. The resonance peak of the parabolic cylinder is much wider than that of the semi-circular cylinder, suggesting some interaction between the vortex wake and the afterbody of the parabolic cylinder.
4. The parabolic cylinder with its elastic axis downstream of its centre of gravity behaves like a soft oscillator, galloping from rest. In the present experiments in smooth flow, the onset of galloping occurred at a reduced velocity of about 6.0. However, the galloping velocity is expected to be dependent upon a number of factors, such as damping, mass ratio, turbulence level and the distance of the elastic axis downstream of the centre of gravity.

Acknowledgements

The authors gratefully acknowledge the financial support of the Natural Sciences and Engineering Research Council (NSERC) of Canada.

References

Blevins, R.D., 1990. Flow-Induced Vibrations, second ed. Van Nostrand Reinhold, New York.

Den Hartog, J.P., 1956. Mechanical Vibrations, forth ed. McGraw-Hill, New York.

Modi, V.J., Slater, J.E., 1983. Unsteady aerodynamics and vortex induced aeroelastic instability of a structural angle section. Journal of Wind Engineering and Industrial Aerodynamics 11, 321–334.

Modi, V.J., Slater, J.E., 1994. Unsteady aerodynamics and vortex-induced aeroelastic response of a structural angle section. Journal of Vibration and Acoustics 116, 449–456.

Nakamura, Y., Tomonari, Y., 1977. Galloping of rectangular prisms in a turbulent flow. Journal of Sound and Vibration 52, 233–241.

Nakamura, Y., Yoshimura, T., 1982. Flutter and vortex excitation of rectangular prisms in pure torsion in smooth and turbulent flows. Journal of Sound and Vibration 84, 305–317.

Naudascher, E., Rockwell, D., 1994. Flow-Induced Vibrations: An Engineering Guide. A.A. Balkema, Rotterdam.

Novak, M., 1972. Galloping oscillations of prismatic structures. ASCE Journal of the Engineering Mechanics Division 98, 27–46.

Novak, M., Tanaka, H., 1974. Effect of the turbulence on the galloping instability. ASCE Journal of the Engineering Mechanics Division 100, 27–47.

Veljkovic, I., 2002. Flow-induced vibrations of a rotary mixing blade. M.A.Sc. Thesis, McMaster University, Hamilton, ON, Canada.